ACS NANO
Cite This: ACS Nano 2019, 13, 6998–7009
www.acsnano.org

ARTICLE

Metal Nanowire Felt as a Flow-Through Electrode for High-Productivity Electrochemistry

Myung Jun Kim,[†] Youngran Seo,[‡] Mutya A. Cruz,[†] and Benjamin J. Wiley*[,†]

[†]Department of Chemistry, Duke University, 124 Science Drive, Box 90354, Durham, North Carolina 27708, United States
[‡]Department of Chemistry, University of North Carolina at Chapel Hill, Chapel Hill, North Carolina 27599, United States

Supporting Information

ABSTRACT: Flow-through electrodes such as carbon paper are used in redox flow batteries, water purification, and electroorganic syntheses. This work examines the extent to which reducing the size of the fibers to the nanoscale in a flow-through electrode can increase the productivity of electrochemical processes. A Cu nanowire felt, made from nanowires 45 times smaller than the 10 μm wide fibers in carbon paper, can achieve a productivity 278 times higher than carbon paper for mass-transport-limited reduction of Cu ions. Higher increases in productivity were predicted for the Cu nanowire felt based on the mass-transport-limited current, but Cu ion reduction became charge transfer-limited on Cu nanowire felt at high concentrations and flow rates when the mass-transport-limited current became comparable to the charge transfer-limited current. In comparison, the reaction rate on carbon paper was mass-transport-limited under all concentrations and flow rates because its mass-transport-limited current was much lower than its charge transfer-limited current. Higher volumetric productivities were obtained for the Cu nanowire felt by switching from Cu ion reduction to Alizarin Red S (ARS) reduction, which has a higher reaction rate constant. An electroorganic intramolecular cyclization reaction with Cu nanowire felt achieved a productivity 4.2 times higher than that of carbon paper, although this reaction was also affected by charge transfer kinetics. This work demonstrates that large gains in productivity can be achieved with nanostructured flow-through electrodes, but the potential gains can be limited by the charge transfer kinetics of a reaction.

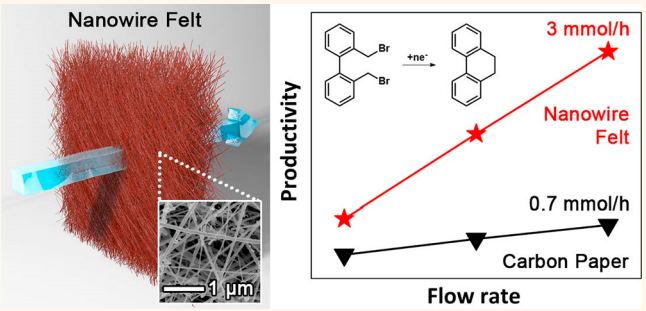

KEYWORDS: *flow electrochemistry, copper nanowires, three-dimensional electrode, flow-through electrode, electroorganic synthesis*

As the percentage of electricity generated from solar power has increased, the periodic curtailment or reduction of output from solar power generators has also increased in order to match supply with demand. For example, the curtailment of renewable power by the California independent system operator (CAISO) has increased from 188 GWh in 2015 to 461 GWh in 2018.[1] Nearly all the renewable power that was curtailed (94%) was from solar rather than wind. Several recent reports indicate solar curtailment occurs because it is the lowest cost solution to manage periodic oversupply of electricity.[2−4] The increasingly large glut of solar power during the day represents an opportunity to use this wasted resource in new electrochemical processes. The use of otherwise wasted solar power for organic electrochemistry would have the twofold benefit of (1) providing an additional revenue stream to solar power generators and (2) replacing toxic oxidants and reducing agents with renewable electricity.

One of the hurdles to increasing the utilization of electricity for chemical production is the volumetric productivity of electrochemical processes (i.e., the production rate of product per unit volume) scales with the surface area of the electrode, rather than the volume of the reactor. As a result, industrial electrochemical reactors tend to be much larger and more expensive than heterogeneous gas-phase or homogeneous chemical reactors for a given rate of chemical production.[5] Partly for this reason, only one (adiponitrile) of the several hundred organic chemicals that are produced at a scale exceeding 10^4 tons per year is made with an electrochemical process.[6] Increasing the volumetric productivity of electrochemical processes, and thus their economic benefits, has long been a central goal of electrochemical engineering.[6]

Received: March 15, 2019
Accepted: May 14, 2019
Published: May 14, 2019

DOI: 10.1021/acsnano.9b02058
ACS Nano 2019, 13, 6998–7009

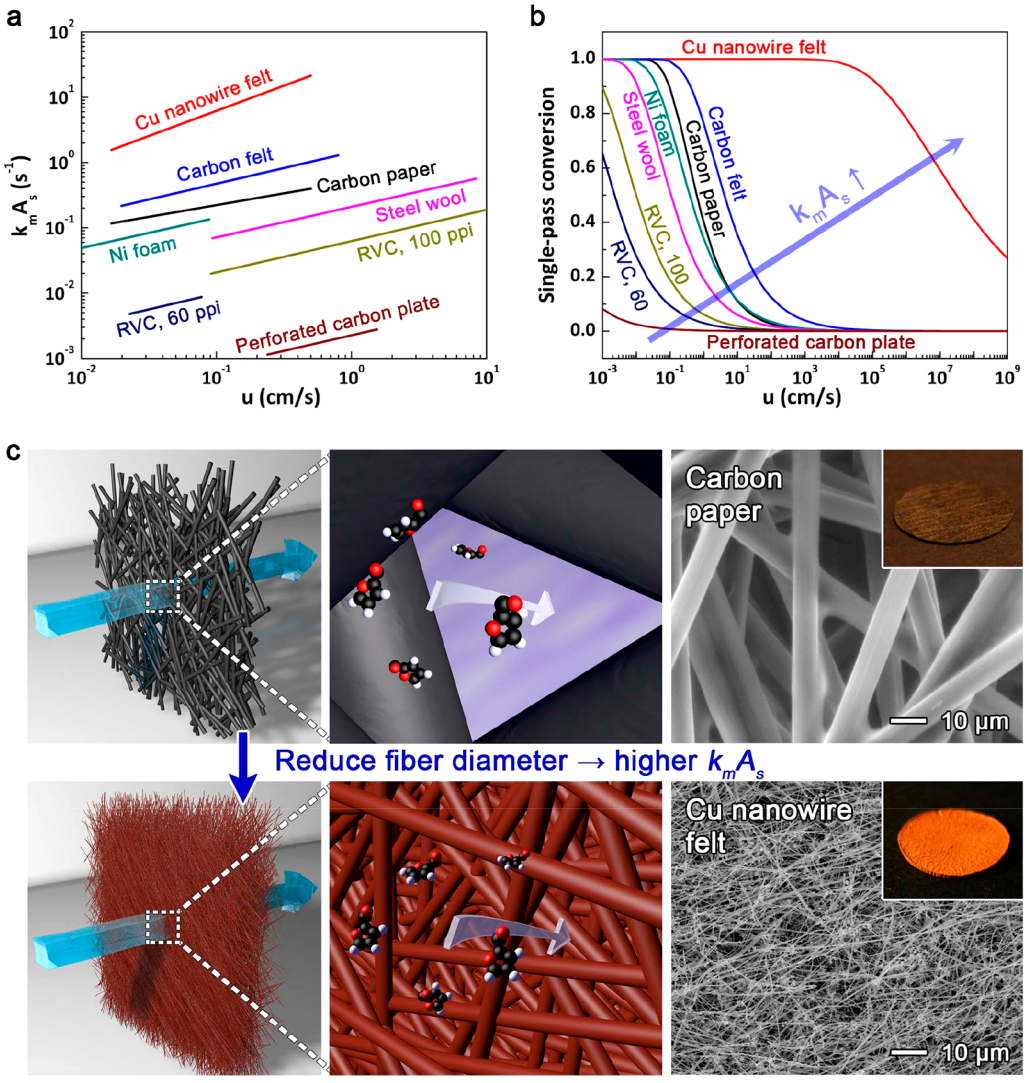

Figure 1. Performance of flow-through electrodes is determined by their specific surface area (A_s) and mass transport coefficient (k_m). (a) Empirical relationship between k_mA_s and u for various flow-through electrodes.[43,44] (b) Associated single-pass conversion for porous electrodes that are 1 cm thick, calculated using eq 1 and the k_mA_s–u functions in Table S2. (c) Schematic illustration of this study's effort to explore how reducing the size of the fibers in a flow-through electrode to the nanoscale can improve productivity. SEM images show the different diameter of the fibers in the Cu nanowire felt and carbon paper. Insets are photographs of the Cu nanowire felt and carbon paper.

At the relatively high voltages and currents used to drive an electrochemical process at its maximum rate, the reaction will usually be limited by mass transport of reactants to the electrode or transport of products away from the electrode (Figure S1). Under such *mass-transport-limited conditions*, the reaction rate is independent of the applied potential or electrode material (i.e., the rate is independent of the electrocatalytic activity). This is in contrast to *charge transfer-limited conditions*, for which the concentration of the reactant at the surface of the electrode is the same as the concentration in the bulk solution, and thus the reaction rate will depend only on the electrode material and the applied potential (Figure S1).

One way to increase the rate of transport of reactants/products to/from an electrode surface, and thereby increase the mass-transport-limited current and productivity, is to use fluid flow.[7,8] Flow electrochemical systems can be categorized as flow-by or flow-through configurations. A flow-by system consists of two parallel electrodes between which the electrolyte flows. For electroorganic syntheses, early flow-by cells with channel lengths of 1−3 cm required flow rates less than 0.1 mL/min to obtain a high single-pass conversion, yielding only a few milligrams of product per hour.[9−11] Electrochemical reactors with long spiral channels up to 2 m in length were subsequently developed to increase production rates to a few grams per hour.[8,12,13] However, the use of 2D planar electrodes requires the reactor have a relatively large volume to achieve a high level of productivity.

An alternative reactor design is a flow-through configuration, in which the electrolyte flows through a three-dimensional (3D) porous electrode.[7,8] The finely divided nature of flow-through electrodes (FTEs) results in more surface area per unit volume than 2D planar electrodes. In addition, FTEs have a higher mass transport coefficient than planar electrodes because the distribution of the electrode surface throughout the reaction solution decreases the distance reactants must travel to reach the electrode surface.[7] Several types of FTEs are commercially available, including carbon paper,[14] graphite felt,[15,16] reticulated vitreous carbon (RVC),[17−19] metal mesh,[20] and metal foam.[21] These electrodes were all developed in the

DOI: 10.1021/acsnano.9b02058
ACS Nano 2019, 13, 6998−7009

1970s or earlier.[22−25] Most efforts to improve the electrochemical performance of flow-through electrodes have focused on the application of surface coatings and treatments to commercially available electrodes.[26−29] Despite the importance of FTEs in a wide variety of electrochemical processes,[30−32] there has been little work devoted to understanding how to create new electrode structures that offer higher productivities than FTEs that were developed 40 years ago.

This study explores what gains in productivity can be achieved through the use of a flow-through electrode made of Cu nanowires (NWs). Cu NWs were used in this study because they can be produced in relatively large scales (4.4 g per batch) at low cost ($5/g),[33] they can be produced to have the desired dimensions,[34] they can be easily annealed together at low temperatures, and they can be coated with noble metals and metal oxides to modify their corrosion resistance and electrocatalytic properties.[35,36] We refer to this electrode as a Cu NW felt because it has a similar porosity to graphite felt. The smaller diameter of the Cu NWs (220 nm) relative to the carbon fibers (10 μm) used in carbon paper leads to a 15-fold increase in the specific surface area. The more finely divided nature of the Cu NW felt relative to carbon paper resulted in an increase in the mass transport coefficient by up to 3.6 times at the highest flow rates. Under mass-transport-limited conditions, the Cu NW felt could reduce Cu ions with a single-pass conversion of 75% at a flow rate 278 times greater than that of carbon paper. The Cu NW felt increased the productivity of an intramolecular cyclization reaction by 4.2 times compared to the carbon paper. This work indicates it is possible to greatly improve the productivity of flow electrochemical processes through the use of nanostructured electrodes with higher specific surface areas and mass transport coefficients.

RESULTS AND DISCUSSION

Performance of Flow-Through Electrodes. The maximum productivity for an electrochemical reactor is determined by its mass-transport-limited current, I_L, which for a flow-through configuration is given by eq 1.[37−39]

$$I_L = nFA_r uC_0\left[1 - \exp\left(-\frac{Lk_mA_s}{u}\right)\right] \quad (1)$$

Here n is the number of electrons required for the reaction, F is the Faraday constant, A_r is the cross-sectional area of the porous electrode, u is the superficial velocity, C_0 is the concentration of reactant at the inlet, L is the thickness of the porous electrode, k_m is the mass transport coefficient, and A_s is the specific surface area. The term inside the brackets gives the single-pass conversion. The term nFA_ruC_0 corresponds to the value of the current at a single-pass conversion of 100%, i.e., the maximum current for a given flow rate, concentration, and electrode diameter. If one fixes the reactor dimensions (L, A_r), the inlet concentration C_0, and the flow rate u, then I_L depends on the k_mA_s of the FTE. This makes k_mA_s an important figure of merit for comparing the performance of different flow-through electrodes. Equation 2 shows that the value of k_mA_s depends on the flow rate u in a functional form that can be derived from the empirical relationship between the Sherwood (Sh), Reynolds (Re), and Schmidt (Sc) numbers (see the Supporting Information and Table S1):[37−42]

$$k_mA_s = au^b \quad (2)$$

Here a and b are empirical constants. Thus, the electrochemical performance of a FTE is determined by how k_mA_s changes with u.

The empirical relationship between k_mA_s and u for various FTEs is shown in Figure 1a and Table S2.[43,44] The corresponding single-pass conversions as a function of flow rate are shown in Figure 1b which were calculated using eq 1 and the k_mA_s−u functions in Table S2. As expected from eq 2, a FTE with a higher k_mA_s results in a higher single-pass conversion. Figure 1 shows previous FTEs have k_mA_s values lower than 1 s^{-1} when u < 10 cm s^{-1}. Low values of k_mA_s limit the flow rate at which a high single-pass conversion can be maintained, and thus limit the productivity of a flow-through electrochemical reactor.

One way to increase the k_mA_s of fibrous electrodes is to use thinner fibers. For an electrode with a given porosity, thinner fibers will increase A_s and decrease the pore size, resulting in a larger k_m. We developed a three-dimensional porous electrode consisting of Cu NWs with diameters of 220 nm (45 times smaller than the 10 μm carbon fibers in carbon paper or graphite felt) to explore the extent to which the use of thinner fibers improves k_mA_s, and thus reactor productivity. Figure 1c illustrates the concept behind this approach, and shows scanning electron microscopy (SEM) images comparing the dimensions of the fibers that make up Cu NW felt and carbon paper. Figure 1 shows the extent to which Cu NW electrodes can increase k_mA_s, and thus the single-pass conversion under mass-transport-limited conditions.

Physical Properties of a Cu NW Felt. The physical properties of the Cu NW felt and other FTEs are summarized in Figure 2 and Table S3. Images for the Cu NWs used in this study and the diffraction pattern of the Cu NW felt are shown in Figure S2. The details of the characterization methods are presented in the Experimental Section. The Cu NW felt was fabricated via vacuum filtration, followed by annealing in H_2 to remove surface oxides and sinter the Cu NWs together. Heating can also partially melt and break NWs,[45] so the annealing temperature was optimized to find the minimum electrical resistivity that results from the trade-off between sintering and melting (Figure S3). At the optimum temperature of 350 °C for 30 min, the electrical resistivity of Cu NWs was 143 $\mu\Omega$·cm, which is 2000 times more conductive than graphite felt and 7 times more conductive than Ni foam. Although the filtered Cu NWs came apart in water before annealing, the annealed Cu NW felt retained its structure and did not collapse under a flow rate of 1 cm/s (Figure S4).

The specific surface area (A_s) of the Cu NW felt was determined with a double-layer capacitance measurement (Figure S5).[46,47] The A_s of 2.38 × 10^4 cm^2/cm^3 is 15 times larger than that of carbon paper and 104 times larger than that of graphite felt. The surface area per unit mass of the Cu NW felt was 4.46 × 10^4 cm^2/g, which was 13 and 8.8 times larger compared to carbon paper and graphite felt, respectively, using the density of the Cu and graphitic carbon. The porosity of the Cu NW felt (94%) was determined from measuring its mass and volume (Figure S6). This porosity can be compared to that predicted by a model developed from measurements of randomly packed rigid cylinders (i.e., uncooked spaghetti).[48] The Cu NWs used for the NW felt have an aspect ratio of 182, for which this model predicts a porosity of 94.3%. As this predicted porosity matches that of the Cu NW felt, we can conclude that the Cu NWs remained as rigid cylinders and were not bent during the fabrication process.

DOI: 10.1021/acsnano.9b02058
ACS Nano 2019, 13, 6998−7009

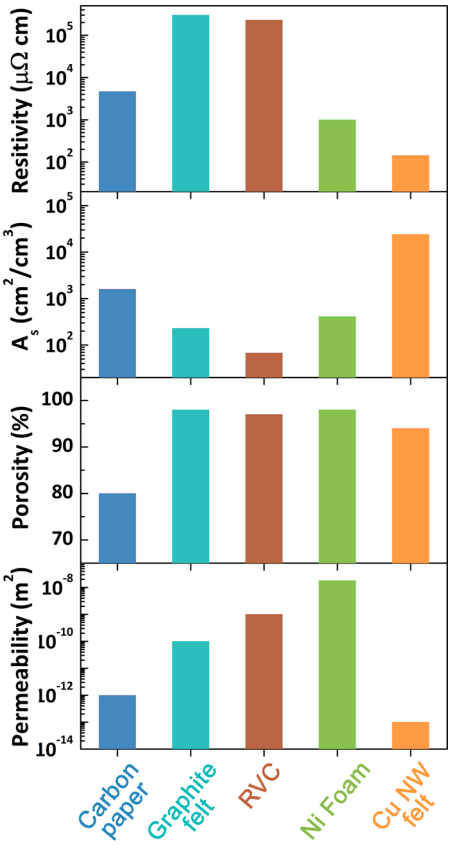

Figure 2. Resistivity, specific surface area (A_s), porosity, and permeability of carbon paper,[52−54] graphite felt,[55] reticulated vitreous carbon (RVC),[18,19,56] Ni foam,[57] and Cu nanowire felt. The values of these properties are summarized in Table S3.

The permeability of the Cu NW felt was determined by applying Darcy's law to measurements of the pressure drop as a function of flow rate (Figure S7).[49−51] The experimental permeability of the Cu NW felt was 9.92×10^{-14} m^2. This permeability can be compared to that predicted by the Kozeny−Carman equation (see eq 7 in Experimental Section). The Kozeny−Carman equation predicts that the permeability will decrease with the square of the fiber diameter, indicating that reducing the diameter of the fibers in a FTE will decrease permeability.[50] At relatively high porosities, values for K_c are 7.1 for flow perpendicular to aligned fibers and 5.7 for flow-through randomly aligned fiber structures.[50] For these K_c values, the Kozeny−Carman equation predicts a permeability for the Cu NW felt of 1.22×10^{-13} and 9.83×10^{-14} m^2, respectively. The measured permeability is between these two values and closer to the value predicted for randomly aligned fiber structures, indicating that the permeability of the Cu NW felt is well-described by previous theories for the permeability of fibrous media.[50] Although the permeability of the Cu NW felt is low relative to other FTEs, it is still sufficient for performing electroorganic synthesis. For example, for the thickness (324 μm) and cross-sectional area (0.5 cm^2) of the Cu NW felt used in this study, the pressure required to achieve a flow rate of 10 cm/s (300 mL/min) is 2.87 atm, which is lower than the typical water pressure in-house (~3 atm).

Electrochemical Performance of Cu NW Felt. Cu ion reduction at three different concentrations was used to determine the k_mA_s and single-pass conversion of the Cu NW felt relative to carbon paper. Carbon paper was chosen for this comparison because it has the largest specific surface area among FTEs that are commercially available. Note that our experiments were performed at mass-transport-limited conditions (Figure S1), meaning that the difference in performance was not due to a difference in the electrocatalytic activity of Cu and carbon. The difference in the electrochemical performance was only due to the structural and dimensional differences between the Cu NW felt and carbon paper. Figure 3 shows the reduction currents were higher for the Cu NW felt relative to carbon paper under all conditions. Equation 1 was

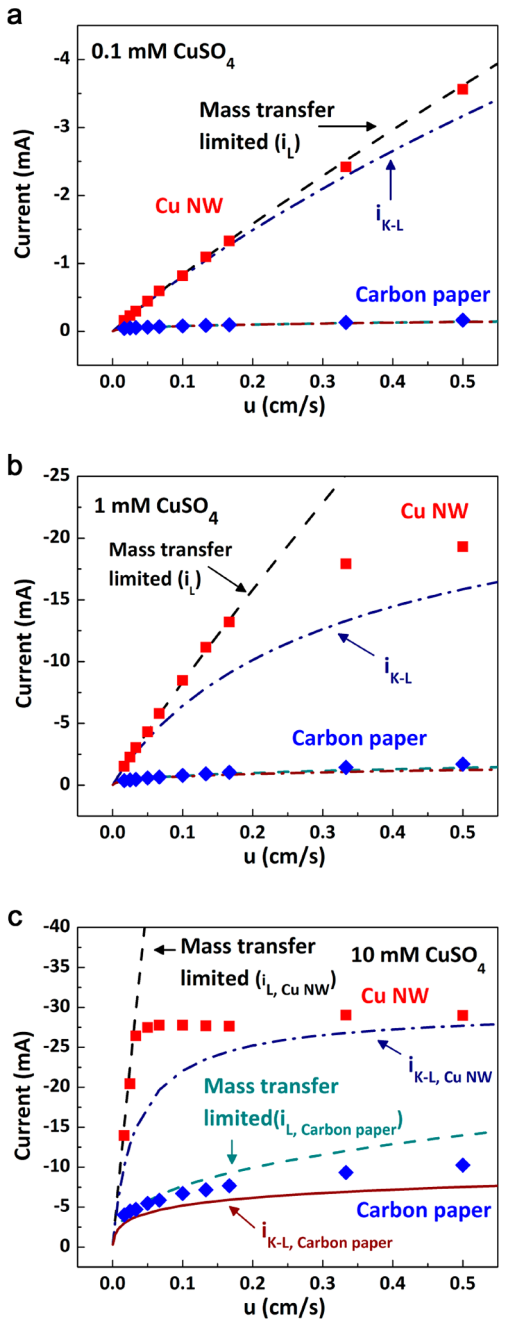

Figure 3. Average current for Cu ion reduction from Cu nanowire felt and carbon paper versus superficial velocity in (a) 0.1 mM, (b) 1 mM, and (c) 10 mM $CuSO_4$ electrolytes. The lines in (a)−(c) correspond to calculated results based on the Koutecký−Levich equation (dash-dot) and the mass-transport-limited current (dash).

DOI: 10.1021/acsnano.9b02058
ACS Nano 2019, 13, 6998−7009

used to solve for the value of k_mA_s for each current measurement in Figure 3 that was mass-transport-limited. These values of k_mA_s can be plotted as a function of u to obtain the empirical correlations shown in Figures 4 and S8. These

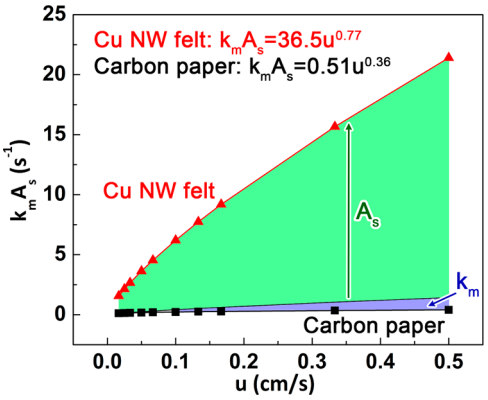

Figure 4. k_mA_s as a function of superficial velocity calculated from the average mass-transport-limited currents. Highlighted areas correspond to the contributions of A_s and k_m to an overall increase in k_mA_s for the Cu NW felt relative to carbon paper.

data show that the Cu NW felt has a k_mA_s value 13.4−53.9 times greater than carbon paper at the same flow rate. Since the A_s of the two electrodes is known, we can further decompose the difference in k_mA_s to contributions from A_s and k_m. Figure 4 shows the difference in k_mA_s is largely due to the difference in the A_s of the two electrodes. The A_s of the Cu NW felt is 15 times higher than carbon paper. The k_m values for both electrodes are similar at low flow rates, and the k_m of the Cu NW felt is as much as 3.6 times greater than the k_m of the carbon paper at the fastest flow rate.

Figure 3 shows that the measured currents for the Cu NW felt deviated from the mass-transport-limited current at higher Cu ion concentrations and higher flow rates. This deviation can also be observed in the single-pass conversion as a function of the flow rates (Figure 5a). Note that the single-pass conversion is independent of the initial Cu ion concentration according to eq 1. The single-pass conversion from carbon paper did not vary significantly with changes in Cu ion concentration, indicating that Cu ion reduction was consistently mass-transport-limited over carbon paper. In contrast, the single-pass conversion for the Cu NW felt was highly dependent on the Cu ion concentration and flow rate (Figure 5a). These data indicate that, as the flow rate and concentration of reactant was increased, the mass transfer-limited current became comparable to the charge transfer-limited current, and charge transfer began to limit the rate of Cu ion reduction at the surface of the electrode. This deviation only occurred for the Cu NW felt because its mass transfer-limited current is much larger than that of carbon paper.

Equation 3, the Koutecký−Levich equation, allows one to incorporate a charge transfer limitation into the prediction of the electrochemical performance of the Cu NW felt.[58]

$$\frac{1}{i_{K-L}} = \frac{1}{i_L} + \frac{1}{i_K} \quad (3)$$

Here, i_{K-L} is the current that results from a mixture of mass transport and charge transfer limitations and i_K is the charge transfer-limited current. The i_K is the current in the absence of any effects from mass transport.[58] The value of i_K is potential-

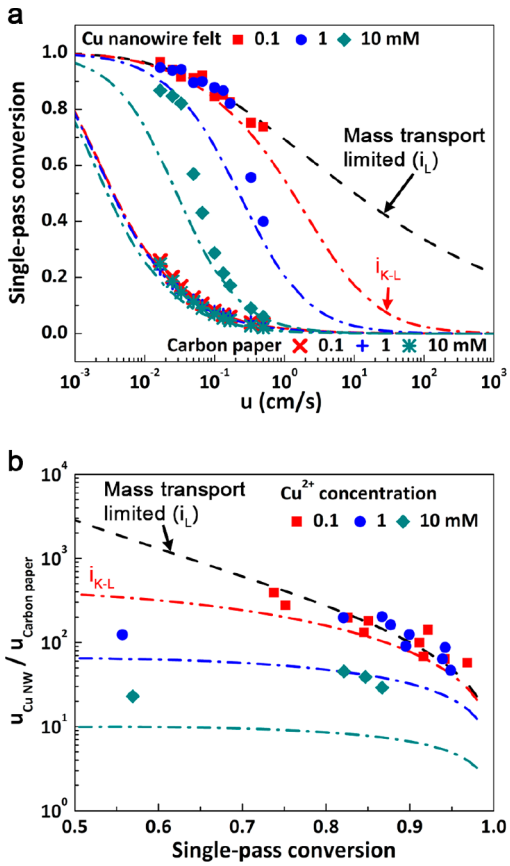

Figure 5. Single-pass conversion and the productivity for Cu nanowire felt and carbon paper. (a) Single pass conversions for reduction of Cu^{2+} at concentration of 0.1, 1, and 10 mM are compared to calculated results based on the Koutecký−Levich equation (i_{K-L}, dash-dot) and the mass-transport-limited current (i_L, dash). (b) Ratio of superficial velocity from Cu nanowire felt and carbon paper at the same single-pass conversion for different concentrations of Cu^{2+}. The symbols in (b) are the experimental results, and the dash-dot lines are calculated using eqs 1 and 3, and the k_mA_s−u correlations for the Cu NW felt and carbon paper.

dependent and will increase linearly with the electrode surface area, the reactant concentration, and the reaction rate constant.[58] No matter how large the value of i_L is, the rate of the electrochemical reaction cannot exceed i_K. Since i_K reflects a situation when the concentration of reactants at the electrode surface is identical to the concentration in the bulk electrolyte, the value of i_K was taken as the current measured at the beginning of chronoamperometry (Table S4). The i_K values in Table S4 were used to calculate the lines for i_{K-L} in Figures 3 and 5a.

Equation 3 indicates that when i_L becomes comparable to i_K, the resulting current will be affected by i_K. Such conditions were not observed for carbon paper because its smaller k_mA_s results in an i_L that was much smaller than i_K in our experiments (Figure 6a). In contrast, the current for Cu NW felt was affected by i_K at higher concentrations and/or flow rates because the i_L was comparable to i_K (Figure 6b). This deviation caused the current and single-pass conversions to deviate from i_L (dash lines) and follow i_{K-L} (dash-dot lines) when $i_L > 0.4i_K$ in Figures 3 and 5a. This result suggests that charge transfer limitations should be considered when calculating what increase in electrochemical performance can be obtained with an FTE that has a large k_mA_s.

DOI: 10.1021/acsnano.9b02058
ACS Nano 2019, 13, 6998−7009

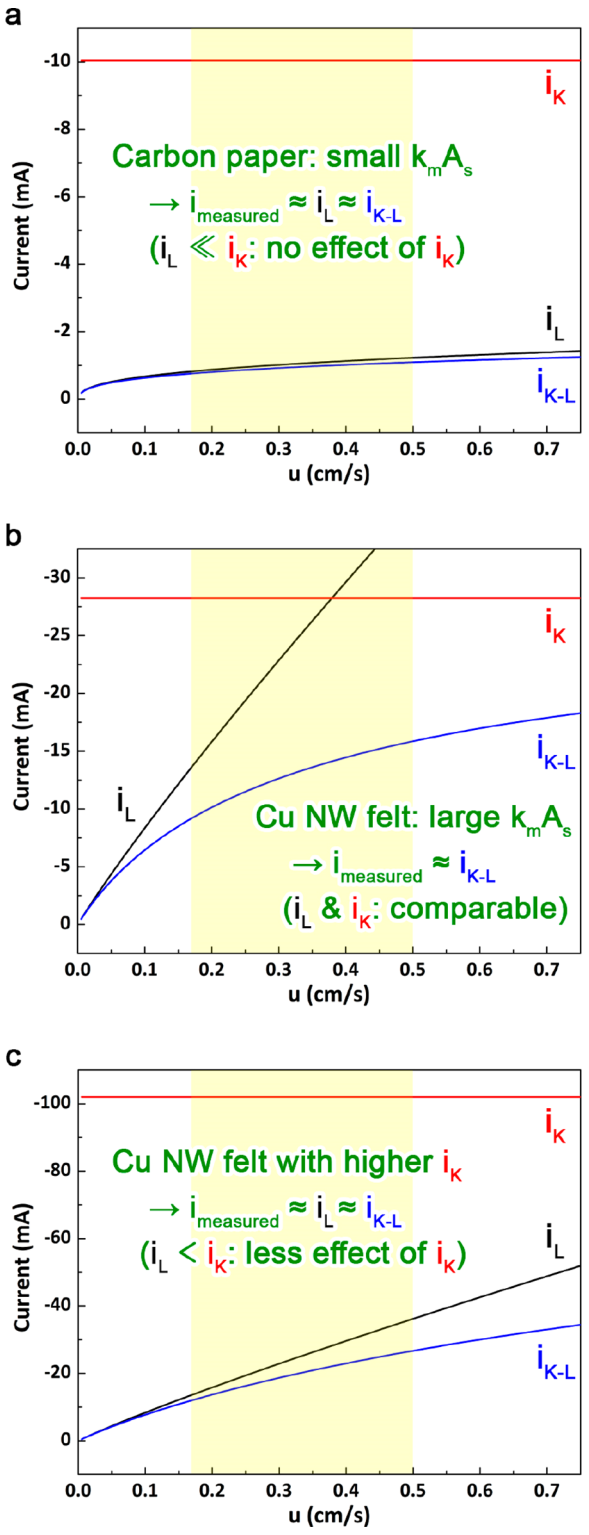

Figure 6. Comparison of i_L, i_K, and i_{K-L} for (a) carbon paper for the reduction of Cu ions and (b,c) Cu NW felt for the reduction of (b) Cu ions and (c) ARS at concentrations of 1 mM. The range of superficial flow rates examined in this study is highlighted in yellow. The lines for i_L and i_{K-L} were calculated using eqs 1 and 3 with the k_mA_s–u relationships in Table S2 and i_K values in Table S4.

The relationship between flow rate and single-pass conversion dictates the productivity of a FTE. In the absence of a charge transfer limitation, the single-pass conversion and productivity can be predicted from eq 1. However, for a FTE with a large k_mA_s value (such as the Cu NW felt), the charge transfer limitation can cause the productivity to deviate from that predicted by eq 1. Figure 5b presents the ratio of flow rates between the Cu NW felt and carbon paper at the same single-pass conversion. Note that the ratio of flow rates in Figure 5b corresponds to the enhancement of the productivity from using a Cu NW felt instead of using carbon paper at the same initial concentration of reactant. At a concentration of 0.1 mM Cu^{2+}, the charge transfer limitation was relatively small, and the productivity for the Cu NW felt electrode was 68 times greater at a single-pass conversion of 0.92, and 278 times greater at a single-pass conversion of 0.75. These values are essentially the same as those predicted by eq 1, indicating the reaction is mass-transport-limited. When charge transfer limited the reaction rate on Cu NW felt but not carbon paper (the 10 mM case), the ratio of the flow rates decreased to 29 times at a single-pass conversion of 0.87 and 22 times at a single-pass conversion of 0.57. In comparison, eq 1 predicts a 1650-fold increase in the productivity of Cu NW felt relative to the carbon paper at a single-pass conversion of 0.57.

Plots such as Figure 3c can also be used to optimize the flow rate for maximizing the productivity of the flow-through electrochemical reactor. The current for reduction of 10 mM of $CuSO_4$ does not increase above a value of 0.05 cm/s because at this point the reaction becomes charge transfer-limited. Since the reaction becomes charge transfer-limited, higher flow rates decrease the single-pass conversion without increasing productivity. Figure S9 plots productivity and single-pass conversion versus flow rate to show the productivity does not increase with flow rate when the reaction becomes charge transfer-limited.

To confirm that the decrease in productivity enhancement at higher Cu^{2+} concentrations and flow rates was due to a charge transfer limitation, we tested a reaction with a higher reaction rate constant. The standard rate constant for the reduction of Cu^{2+} to Cu^{1+} is 1.1×10^{-6} cm/s,[59] whereas the reduction of Alizarin Red S (ARS) has a standard rate constant of 3.6×10^{-3} cm/s (Figure 7a).[60] Note that the relationship between k_mA_s and u will be different between Cu^{2+} and ARS reduction because of the different diffusion coefficients of these reactants. Therefore, the k_mA_s behavior for ARS was measured (Figure S10) in order to calculate i_L and the single-pass conversion in Figure 7b. The higher rate constant for the ARS reduction was reflected in an i_K of −102.1 mA compared to −28.2 mA for the Cu ion reduction at a concentration of 1 mM for both reactants (Table S4). As shown in Figure 7b, the higher i_K for ARS reduction allowed the single-pass conversion to match the values predicted from i_L, while at the same flow rate and concentration, the single-pass conversion from Cu ion reduction exhibited a transition from i_L to i_{K-L} (see also Figure 6b and c).

The productivity shown in Figure 7c further illustrates the effect of the rate constant on the performance of the Cu NW felt. At a lower flow rate, the productivities of Cu^{2+} and ARS reduction were similar because both reactions were mass-transport-limited. At higher flow rates (15 mL/min), the productivities diverged due to the faster charge transfer kinetics for ARS reduction. The productivity for the Cu^{2+} reduction over Cu NW felt was 11 times higher compared to carbon paper, whereas the productivity for ARS reduction over Cu NW felt was 19 times higher. These results illustrate that a

DOI: 10.1021/acsnano.9b02058
ACS Nano 2019, 13, 6998−7009

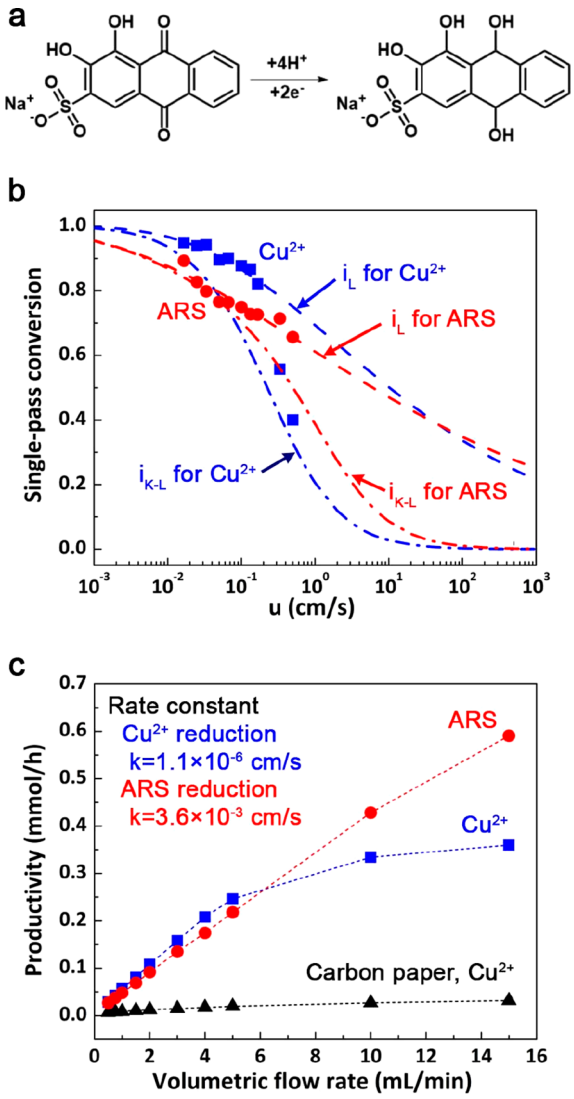

Figure 7. Effect of i_K on the performance of Cu nanowire felt. (a) Scheme for ARS reduction. (b) Single-pass conversion and (c) productivity for the reduction of Cu ions and ARS as a function of flow rate.

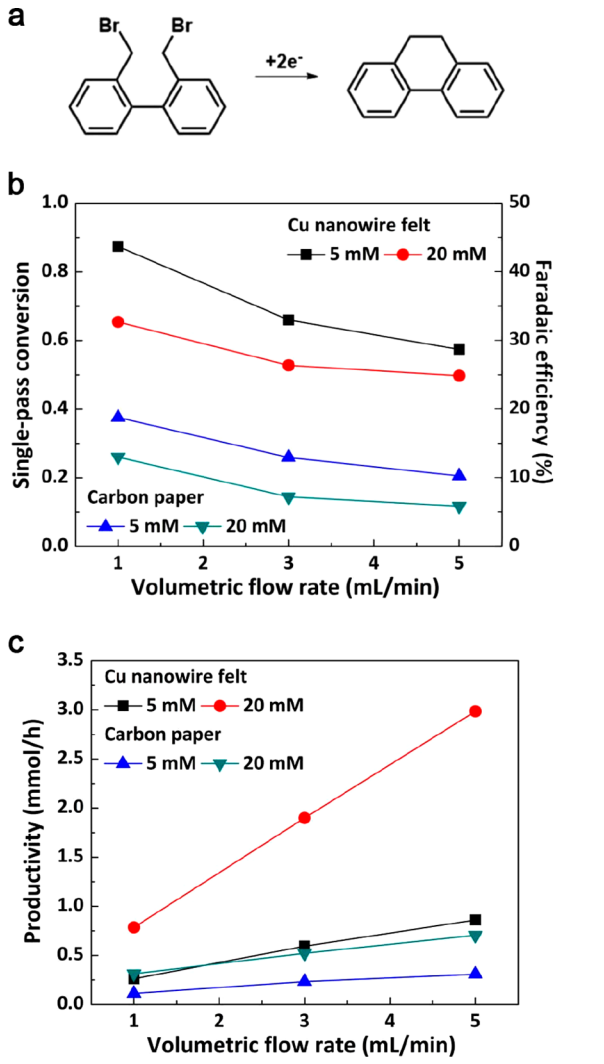

Figure 8. (a) Scheme for conversion of 2,2′-bis(bromomethyl)-1,1′-biphenyl to 9,10-dihydrophenanthrene. (b) Single-pass conversion, Faradaic efficiency, and (c) corresponding productivity of 9,10-dihydrophenanthrene as a function of volumetric flow rate and concentration of 2,2′-bis(bromomethyl)-1,1′-biphenyl for Cu nanowire felt and carbon paper.

reaction with a higher rate constant will benefit the most from the use of a nanostructured FTE.

Electrochemical Reduction of 2,2′-Bis(bromomethyl)-1,1′-biphenyl. To test the suitability of the Cu NW felt for electroorganic synthesis, we studied the intramolecular cyclization of 2,2′-bis(bromomethyl)-1,1′-biphenyl to produce 9,10-dihydrophenanthrene via electrochemical reductive dehalogenation (Figure 8a). This intramolecular cyclization was performed galvanostatically in an undivided flow cell (Figure S11b) with the Cu NW felt or carbon paper as the working electrode. The reduction current was first varied to maximize the single-pass conversion at a reactant concentration of 5 mM and a flow rate of 1 mL/min (Figure S12). The highest single-pass conversion (0.87) was obtained at a current of 32 mA, corresponding to four electrons per molecule. In comparison, the theoretical number of electrons required per molecule for this intramolecular cyclization is two, so more than two electrons per molecule of product were consumed by side reactions. Although providing a high number of electrons per molecule will increase side reactions, it also increases the likelihood that the concentration of reactants at the surface will be depleted relative to the bulk, resulting in a mass-transport limited condition that maximizes the single-pass conversion for each electrode. Therefore, this ratio of electrons per molecule was kept constant in subsequent experiments in which the concentration of the starting material and the flow rate were varied. SEM images before and after the reaction for 50 min (Figure S13) show no change in the structure of the Cu NW felt, suggesting it is stable under these reaction conditions.

The changes in the single-pass conversion for this reaction as a function of the reactant concentration and flow rate are presented in Figure 8b. Note that the Faradaic efficiency = (single-pass conversion)/2 for this study because we applied twice the theoretical current than was needed to obtain a single-pass conversion of 100%. As expected from eq 1, the single-pass conversion decreased with flow rate for both the Cu NW felt and carbon paper, and the single-pass conversion for the Cu NW felt was significantly higher than that of carbon paper. The Cu NW felt achieved single-pass conversions above 0.58 at 5 mM and above 0.50 at 20 mM at a flow rate of 5 mL/

DOI: 10.1021/acsnano.9b02058
ACS Nano 2019, 13, 6998−7009

min, whereas the maximum conversion obtained with carbon paper was 0.21 at 5 mM and 0.12 at 20 mM at the same flow rate. The improvement in single-pass conversion was due to the higher k_mA_s of the Cu NW felt. The fact that the single-pass conversion decreased as the concentration of reactant increased indicates this reaction was also limited by charge transfer.

Corresponding productivity values for different reaction conditions are summarized in Figure 8c. The maximum productivity for the Cu NW felt (3 mmol/h or 0.54 g/h at a single-pass conversion of 0.5) was 4.2 times higher than that of carbon paper (0.7 mmol/h or 0.126 g/h at a single-pass conversion of 0.12). We also note that the greater single-pass conversion for the Cu NW felt resulted in a productivity at 5 mM that was similar to that of carbon paper at 20 mM. This result illustrates the ability of the NW felt to produce the same quantity of product with 4 times less starting reagent and 4 times lower electrical current for this reaction, thereby reducing the material and energy cost of this electroorganic synthesis. This improvement in Faradaic efficiency for the Cu NW felt was due to an increase in the probability of reactants encountering the electrode surface, leading to an increase in Faradaic efficiency and a decrease in side reactions. For example, at a flow rate of 3 mL/min and an inlet concentration of 5 mM, the Faradaic efficiency was 33% for the Cu NW felts and 13% for carbon paper. These results clearly indicate that a NW felt with a higher k_mA_s value has the potential to make electroorganic synthesis more productive, more green, and more cost-effective.

CONCLUSIONS

This work demonstrates the extent to which decreasing fiber diameter and pore size can increase the k_mA_s of flow-through electrodes, and thereby increase the productivity of electrochemical reactors. Decreasing the diameter of the constituent fibers in the porous electrodes from 10 μm for carbon fiber to 220 nm for Cu NW Felt increased the k_mA_s of the electrodes up to 53.9-fold. The higher k_mA_s translated into a 278-fold productivity increase for the reduction of 0.1 mM Cu^{2+} at a single-pass conversion of 0.75. At higher Cu ion concentrations (e.g., 10 mM), the magnitude of the mass-transport-limited current became large relative to charge transfer-limited current for the Cu NW felt (but not carbon paper), and the productivity enhancement decreased. A comparison of Cu ion and ARS reduction reactions illustrates that the Cu NW felt and similar nanostructured electrodes will provide the greatest increase in productivity for reactions with large reaction rate constants. Lastly, for an intramolecular cyclization limited by mass and charge transport kinetics, a Cu NW felt with a cross-sectional area of only 0.5 cm^2 exhibited a productivity of 3 mmol/h (0.54 g/h), 4.3 times higher than carbon paper. Productivities beyond the g/h scale can thus be achieved by slightly increasing the cross-sectional area of the electrode. A disadvantage of Cu is that it will dissolve under anodic conditions. Future work will focus on development of nanostructured FTEs to achieve both high durability and high k_mA_s. In addition, further research is necessary to improve the Faradaic efficiency of electroorganic syntheses by optimizing reaction conditions and electrode design. We hope this work inspires other nanomaterials researchers to develop novel nanostructured FTEs to improve the efficiency and productivity of flow electrochemical systems.

EXPERIMENTAL SECTION

Synthesis of Cu NWs and Fabrication of the Porous Felt. Cu NWs were synthesized with an ethylenediamine (EDA)-NaOH-based method in which EDA acts as a facet-dependent promoter of Cu NW growth.[33,61] The reaction solution was prepared by sequentially adding the following aqueous solutions to a 2 L glass bottle and shaking vigorously after every addition: (1) 1500 mL of 8 M NaOH (NOAH Technologies, 99%), (2) 160 mL of 0.1 M $Cu(NO_3)_2$ (Sigma-Aldrich, 98%), (3) 23 mL of EDA (Acros Organics, 99%), and (4) 150 mL of 1 g/mL α-D-glucose (Sigma-Aldrich, 96%). The final concentrations of NaOH, $Cu(NO_3)_2$, EDA, and glucose were 6.5 M, 8.73 mM, 186 mM, and 450 mM, respectively. After mixing the solutions, the glass bottle was immediately placed in a 60 °C oven for 4 h. After the reaction, Cu NWs were cleaned with and stored in an aqueous solution containing 3 wt % polyvinylpyrrolidone (PVP, MW = 10,000, Sigma-Aldrich) and 1 wt % *N*,*N*-diethylhydroxylamine (DEHA, TCI, 98%). The average diameter of the synthesized Cu NWs was measured from images obtained using a field emission scanning electron microscope (FEI XL30 SEM-FEG), and the lengths were measured with a dark field optical microscope (DFOM, BX51, Olympus). The average diameter and length of the Cu NWs were 220 ± 70 nm and 40 ± 13 μm, respectively (Figure S2). The concentration of Cu NWs in the storage solution was measured by atomic absorption spectroscopy (AAS, 3100 PerkinElmer).

Prior to the fabrication of the NW felt, Cu NWs in the storage solution were washed three times with isopropyl alcohol (IPA, VWR) by centrifugation and removal of supernatant. The Cu NWs were redispersed in IPA and filtered onto a stainless steel wire cloth (400 mesh, McMaster). The filtration area, 1.13 cm^2, was defined by a silicone gasket (thickness: 508 μm, FuelCellStore) cut with a laser cutter. After filtration, the Cu NW felt was annealed at various temperatures for 30 min under H_2. The optimum temperature for annealing (350 °C) minimized the electrical resistivity of the Cu NW felt (Figure S3). The optimization of annealing temperature was carried out with a 324 μm thick Cu NW felt. The electrical resistivity was calculated from the sheet resistance as measured with a four-point probe, and the thickness was measured with SEM. The diffraction pattern of the Cu NW felt was obtained with an X-ray diffractometer (Panalytical X'Pert Pro).

Flow Cells for Cu Ion Reduction, ARS Reduction, and Organic Electrosynthesis. Two flow cells were fabricated: one with 3D printing and one by machining. The 3D printed undivided flow cell (Figure S11a) was used to measure water permeability and the reduction of Cu ions and Alizarin Red S (ARS). This flow cell was made of polyethylene terephthalate glycol (PETG, Hatchbox), which was chosen for its adequate resistance to the sulfuric acid–based electrolytes used during electrochemical reduction. This flow cell consisted of two parts, an inlet and an outlet. The porous electrode was sandwiched between these parts with two gaskets having a 0.5 cm^2 hole in the center, i.e., the cross-sectional area of the working electrode exposed to liquid flow, giving the following structure: inlet/gasket/electrode/metal mesh/gasket/outlet. The size of the filtered electrode (1.13 cm^2) was larger than the size of the hole of the gasket, so the outer part of the electrode was compressed by the gasket to make a robust electrical contact to a stainless steel wire cloth that was placed downstream of the electrode and was connected to a potentiostat. The metal mesh also provided mechanical support for the Cu NW felts. Cu NW felt (cross-sectional area: 0.5 cm^2) supported by metal mesh could withstand liquid flow at a pressure of at least 0.27 atm as shown in Figure S4. The outlet component had two holes for the reference and counter electrodes. For the measurement of permeability, the outlet component did not have the two holes for the reference and counter electrodes.

Since PETG dissolves in organic solvents, a flow cell for organic synthesis (Figure S11b) was fabricated by machining polyether ether ketone (PEEK). The inlet and outlet pieces were threaded for connection to a perfluoroalkoxy alkane (PFA) compression fitting (McMaster). The flow-through electrode was sandwiched between two Teflon gaskets with a diameter of 0.8 cm. The cross-sectional area

DOI: 10.1021/acsnano.9b02058
ACS Nano 2019, 13, 6998–7009

of the working electrode exposed for liquid flow, which was determined by the hole of the PEEK cell, was 0.5 cm^2 (diameter: 0.8 cm).

Measurement of Physical Properties of the Cu NW Felt. The specific surface area (A_s) of the Cu NW felt was measured with cyclic voltammetry (CV) in 0.1 M $HClO_4$ (VWR, 70%) aqueous solution.[46,47] The solution was purged with N_2 for 30 min prior to the measurements. CV was performed with a potentiostat (CHI600D, CH Instruments, Inc.) and the electrochemical flow cell shown in Figure S11a. The working, reference, and counter electrodes were a 324 μm thick Cu NW felt, a Ag/AgCl electrode (CH Instruments, Inc.), and a Pt mesh, respectively. A stainless steel wire cloth (400 mesh) was placed downstream of the Cu NW felt, and the mesh was connected to a potentiostat. Before starting the measurement, the electrolyte was pumped into the Cu NW felt with a syringe pump (PHD-2000, Harvard Apparatus) to remove the entrapped air. CV was performed with a potential between 0 V and −0.3 V with respect to a Ag/AgCl reference electrode (Figure S5). The capacitive current ($i_{capacitive}$) was measured at −0.15 V while varying the scan rates. The surface area (A) was calculated with eq 4,

$$i_{capacitive} = AC_d\nu \tag{4}$$

where C_d is the capacitance (28 $\mu F/cm^2$)[46,47] for the double layer on a smooth Cu surface in 0.1 M $HClO_4$ and ν is scan rate (mV/s). The surface area calculated using C_d (10.781 mF for Cu NW felt) was 385 cm^2. As the volume of the Cu NW felt was 0.0162 cm^3 (area, 0.5 cm^2; thickness, 0.0324 cm), the specific surface area (A_s) was 2.4×10^4 cm^2/cm^3.

The porosity (ε) of Cu NW felt was obtained from the weight (W_{CuNW}) of electrodes with different thicknesses (Figure S6). The porosity can be calculated using eq 5,

$$\varepsilon = \frac{V_{void}}{V_{total}} = \frac{V_{total} - V_{CuNW}}{V_{total}} = \frac{V_{total} - W_{CuNW}/\rho_{Cu}}{V_{total}} \tag{5}$$

where V_{total} is the volume of the electrode, V_{void} is the volume of the void, and ρ_{Cu} is the bulk density of Cu. W_{CuNW} was measured after filtration and annealing. The area of the filtered electrode was 1.13 cm^2. This area was used to calculate the volume of the electrode along with the thickness measured by SEM. The porosity of the Cu NW felt was found to be 0.94 for thicknesses between 60 and 530 μm (Figure S6).

The permeability of a porous electrode determines the flow rate of electrolyte for a given applied pressure. To determine the permeability of the Cu NW felt, we measured the pressure drop across the electrode as a function of flow rate (Figure S7). The flow rate of water was controlled by a peristaltic pump (VWR), and the corresponding pressure was measured with a pressure gauge (DPGW-05, Dwyer Instruments, Inc.) at the inlet of the flow cell. For laminar flow, the permeability of a porous electrode can be calculated from Darcy's law with eq 6,[49−51]

$$u = -\frac{k}{\mu}\frac{\Delta p}{L} \tag{6}$$

where u is the superficial velocity, k is the permeability, μ is the viscosity of water, and L is the thickness of the electrode. The experimental conditions examined in this study were in the laminar flow regime (Re < 0.04), so Darcy's law was valid. The viscosity of water for the calculation was 8.9×10^{-4} Pa s.

Since the highest Re (ud/ν, where ν is the kinematic viscosity) for the conditions examined in this study was 0.0011 (laminar flow regime), the permeability (k) can be calculated from the porosity (ε) and the diameter of the fibers (d) with the Kozeny−Carman equation as follows,

$$k = \frac{d^2\varepsilon^3}{16K_C(1-\varepsilon)^2} \tag{7}$$

where K_c, the Kozeny constant, is a function of the tortuosity and pore geometry.[50]

Electrochemical Measurements for Cu Ion Reduction and ARS Reduction. The reduction of Cu ions as a function of flow rate was investigated using the flow cell shown in Figure S11a. The electrochemical measurements were carried out with a potentiostat (CHI600D, CH Instruments, Inc.). The aqueous electrolyte was composed of 0.1, 1, and 10 mM $CuSO_4$ (Acros Organics, 99%), 1 M Na_2SO_4 (Alfa Aesar, 99%), and 1 mM H_2SO_4 (VWR, 95−98%). The electrolytes were purged with N_2 for 30 min before performing the electrochemical measurements. The flow rate of electrolyte into the porous electrode was controlled from 0.5 to 15 mL/min with a syringe pump. The working electrodes were Cu NW felt (324 μm) and carbon paper (370 μm, Toray carbon paper 120). Stainless steel wire cloth (400 mesh) was used to electrically connect both electrodes to the potentiostat. The counter and reference electrodes were a Pt mesh and Ag/AgCl electrode (1 M KCl, CH Instruments, Inc.), respectively. The three-electrode system and supporting electrolyte minimized the ohmic drop, enabling accurate measurements of the performance of the porous electrodes.

To determine the potential where the electrochemical reaction is mass-transport-limited and H_2 evolution is minimized, linear sweep voltammetry (LSV) was performed at a scan rate of 20 mV/s. As shown in Figure S14a, the appropriate potential for the reduction of Cu ions under mass-transport-limited conditions was −0.35 V vs Ag/AgCl. The reduction current was recorded by chronoamperometry for 60 s and the average current (i_{avg}) was obtained from the current between 30 and 60 s. Chronoamperometry was also performed in an aqueous solution with 1 M Na_2SO_4 and 1 mM H_2SO_4 to obtain the background current ($i_{background}$). The average background current was subtracted from the average reduction current obtained with Cu ions (Figure S14b), and the single-pass conversion was calculated using the following eq 8.

$$\text{single-pass conversion} = \frac{i_{avg} - i_{background}}{nFA_r uC_0} \tag{8}$$

Here n is the number of electrons required for the reaction, F is the Faraday constant, A_r is the cross-sectional area of the porous electrode, u is the superficial velocity, and C_0 is the concentration of the reactant at the inlet. To minimize the change in surface area due to Cu deposition, a fresh electrode was used for each measurement. Stable current−time profiles were obtained for each measurement (Figure S14b), indicating that structure of the electrodes did not change over the course of the measurement. Furthermore, at the highest reduction current (~28.2 mA), Cu deposition for 60 s would fill only 0.41 vol % of the void volume in the Cu NW felts. Thus, the Cu electrodeposition over the course of the measurements had a negligible effect on the specific surface area and porosity of the Cu NW felts.

The experimental setup for ARS reduction was identical to that of Cu ion reduction. The aqueous electrolyte for ARS reduction consisted of 1 mM ARS (Acros Organics) and 1 M H_2SO_4. The applied potential for chronoamperometry was determined by LSV, and was found to be −0.4 V vs Ag/AgCl (Figure S10a). The method for subtracting the background current was the same as that used for Cu ion reduction.

Electrochemical Reduction of 2,2′-Bis(bromomethyl)-1,1′-biphenyl. Electrochemical reduction of 2,2′-bis(bromomethyl)-1,1′-biphenyl (Sigma-Aldrich) was performed galvanostatically with the PEEK flow cell shown in Figure S11b. The two-electrode system consisted of the Cu NW felt or carbon paper as the cathode and a Zn wire (Alfa Aesar) as the sacrificial anode. Electrical contact was made with a stainless steel wire cloth (400 mesh). The solvent was dimethylformamide (DMF, VWR), and 0.1 M tetraethylammonium p-toluenesulfonate (TCI) was added as the supporting electrolyte. A syringe pump was used to control the flow rate, and a DC power supply (KORAD KA3005P) was used to apply a constant current. The current for the reduction of 2,2′-bis(bromomethyl)-1,1′-biphenyl to 9,10-dihydrophenanthrene was first optimized to maximize the single-pass conversion (Figure S12). The maximum single-pass conversion was observed at a current of 32 mA when the initial

DOI: 10.1021/acsnano.9b02058
ACS Nano 2019, 13, 6998−7009

concentration of 2,2′-bis(bromomethyl)-1,1′-biphenyl and the volumetric flow rate were 5 mM and 1 mL/min, respectively. The currents used in the subsequent experiments testing the effects of flow rate and concentration were calculated to have the same proportion to the molar flow rate of 2,2′-bis(bromomethyl)-1,1′-biphenyl. For example, the applied current with 20 mM 2,2′-bis(bromomethyl)-1,1′-biphenyl at 5 mL/min was 640 mA.

The effluent from the PEEK reactor (Figure S11b) was collected in a glass vial, and the product, 9,10-dihydrophenanthrene, was separated from the effluent via extraction and column chromatography. The effluent (12 mL) was transferred to a separatory funnel with a syringe, and the syringe was rinsed with hexanes (2 mL × 2) into the funnel. After the addition of deionized water (10 mL) to the funnel, the reaction mixture was extracted with hexanes (50 mL × 3). The combined organic layer was washed with deionized water (20 mL), dried over $MgSO_4$, filtered, and concentrated under reduced pressure. The product was purified by silica gel chromatography (10 × 1 cm column) using a gradient elution profile (100% hexanes to 100:1 to 80:1, hexanes:diethyl ether) to obtain 9,10-dihydrophenanthrene. Column chromatography was performed with SiliaFlash P60 40−64 μm (230−400 mesh). All volumes for flash chromatography are reported as v/v. Thin layer chromatography (TLC) was performed on SiliCycle Silica Gel 60 F254 plates and visualized with UV light (254 nm). All nuclear magnetic resonance (NMR) spectra were recorded on a Bruker Avance 600 MHz at standard temperature and pressure (Figure S15). Deuterated chloroform ($CDCl_3$) was used as received from Cambridge Isotope Laboratories, Inc. The residual solvent proton (^1H) or the solvent carbons (^{13}C) were used as internal references (7.26 ppm for ^1H NMR, 77.16 ppm for ^{13}C NMR). ^1H NMR data was reported as follows: chemical shift (multiplicity, coupling constant, integration). The abbreviations for multiplicity s, d, and m correspond to singlet, doublet, and multiplet, respectively. The single-pass conversion was calculated from the isolated yield obtained from the weight of 9,10-dihydrophenanthrene.

9,10-Dihydrophenanthrene:[62] Clear oil film; ^1H NMR (600 MHz, $CDCl_3$) δ 7.78 (d, J = 7.7 Hz, 2H), 7.34−7.31 (m, 2H), 7.29−7.22 (m, 4H), 2.90 (s, 4H); ^{13}C NMR (151 MHz, $CDCl_3$) δ 137.5, 134.6, 128.3, 127.5, 127.1, 123.8, 29.2.

ASSOCIATED CONTENT

Supporting Information

The Supporting Information is available free of charge on the ACS Publications website at DOI: 10.1021/acsnano.9b02058.

Derivation of the k_mA_s−u relationship from dimensionless numbers; current−potential curves for three arbitrary electrodes with different electrocatalytic activities; SEM and DFOM images of Cu NWs; XRD pattern for the Cu NW felt; electrical resistivity of the Cu NW felts with different annealing temperatures; cross-sectional images of an annealed Cu NW felt before and after liquid flow; electrochemical measurements to determine the specific surface area of Cu NW felt; thickness−weight relationship used to determine the porosity of the Cu NW felts; measurement of permeability; k_mA_s−u relationship for Cu NW felt and carbon paper; productivity and single-pass conversion for Cu ion reduction with Cu NW felts; additional electrochemical measurements for Cu ion and ARS reduction; pictures of two flow cells; single-pass conversion for reductive dehalogenation with different applied currents; SEM images of the Cu NW felt before and after electroorganic synthesis; NMR spectra of 9,10-dihydrophenanthrene; dimensionless numbers used in the k_mA_s−u relationship; equations for the k_mA_s−u relationship; physical properties for various porous electrodes; charge transfer-limited currents for Cu ion and ARS reduction with Cu NW felt and carbon paper (PDF)

AUTHOR INFORMATION

Corresponding Author

*E-mail: benjamin.wiley@duke.edu.

ORCID

Myung Jun Kim: 0000-0002-9056-4904

Benjamin J. Wiley: 0000-0002-1314-6223

Notes

This work was posted to ChemRxiv.[63]

The authors declare no competing financial interest.

ACKNOWLEDGMENTS

This work was supported by an ACS GCI Pharmaceutical Roundtable Research Grant, a National Science Foundation CAREER award (DMR-1253534), and a grant from the Duke University Energy Initiative.

REFERENCES

(1) Wind and Solar Curtailment Totals by Month, California Independent System Operator. http://www.caiso.com/Style%20Library/caiso/csv/curtailmentsMonthly.csv (accessed January 2019).

(2) Proposed Reference System Plan, Modeling Results Files and RESOLVE Model. California Public Utilities Commission, September 2017, http://cpuc.ca.gov/irp/proposedrsp/ (accessed January 2019).

(3) Solar Potential Analysis Report, Clean Power Research. November 2018, http://mnsolarpathways.org/spa/ (accessed January 2019).

(4) Investigating the Economic Value of Flexible Solar Power Plant Operation. Energy and Environmental Economics, Inc., October 2018, https://www.ethree.com/wp-content/uploads/2018/10/Investigating-the-Economic-Value-of-Flexible-Solar-Power-Plant-Operation.pdf (accessed January 2019).

(5) Roberts, R.; Ouellette, R. P.; Cheremisinoff, P. N. *Industrial Applications of Electroorganic Synthesis*; Ann Arbor Science: Ann Arbor, MI, 1982; pp 171−174.

(6) Pletcher, D.; Walsh, F. C. *Industrial Electrochemistry*, 2nd ed.; Springer Science & Business Media, 2012; pp 294−330.

(7) Pletcher, D.; Green, R. A.; Brown, R. C. D. Flow Electrolysis Cells for the Synthetic Organic Chemistry Laboratory. *Chem. Rev.* **2018**, *118*, 4573−4591.

(8) Green, R. A.; Brown, R. C. D.; Pletcher, D. Electrosynthesis in Extended Channel Length Microfluidic Electrolysis Cells. *J. Flow Chem.* **2016**, *6*, 191−197.

(9) Suga, S.; Okajima, M.; Fujiwara, K.; Yoshida, J. "Cation Flow" Method: A New Approach to Conventional and Combinatorial Organic Syntheses Using Electrochemical Microflow Systems. *J. Am. Chem. Soc.* **2001**, *123*, 7941−7942.

(10) Horii, D.; Atobe, M.; Fuchigami, T.; Marken, F. Self-Supported Methoxylation and Acetoxylation Electrosynthesis Using a Simple Thin-Layer Flow Cell. *J. Electrochem. Soc.* **2006**, *153*, D143−D147.

(11) Kashiwagi, T.; Amemiya, F.; Fuchigami, T.; Atobe, M. *In Situ* Electrogeneration of O-Benzoquinone and High Yield Reaction with Benzenethiols in a Microflow System. *Chem. Commun.* **2012**, *48*, 2806−2808.

(12) Green, R. A.; Brown, R. C. D.; Pletcher, D.; Harji, B. An Extended Channel Length Microflow Electrolysis Cell for Convenient Laboratory Synthesis. *Electrochem. Commun.* **2016**, *73*, 63−66.

(13) Green, R. A.; Jolley, K. E.; Al-Hadedi, A. A. M.; Pletcher, D.; Harrowven, D. C.; De Frutos, O.; Mateos, C.; Klauber, D. J.; Rincón, J. A.; Brown, R. C. D. Electrochemical Deprotection of Para-Methoxybenzyl Ethers in a Flow Electrolysis Cell. *Org. Lett.* **2017**, *19*, 2050−2053.

DOI: 10.1021/acsnano.9b02058
ACS Nano 2019, 13, 6998−7009

(14) Kordesch, K.; Jahangir, S.; Schautz, M. Engineering Concepts and Technical Performance of Oxygen-Reducing Electrodes for Batteries and Electrochemical Processes. *Electrochim. Acta* **1984**, *29*, 1589−1596.
(15) Kinoshita, K.; Leach, S. C. Mass-Transfer Study of Carbon Felt, Flow-Through Electrode. *J. Electrochem. Soc.* **1982**, *129*, 1993−1997.
(16) Oren, Y.; Soffer, A. Graphite Felt as an Efficient Porous Electrode for Impurity Removal and Recovery of Metals. *Electrochim. Acta* **1983**, *28*, 1649−1654.
(17) Blaedel, W. J.; Wang, J. Flow Electrolysis on a Reticulated Vitreous Carbon Electrode. *Anal. Chem.* **1979**, *51*, 799−802.
(18) Strohl, A. N.; Curran, D. J. Reticulated Vitreous Carbon Flow-Through Electrodes. *Anal. Chem.* **1979**, *51*, 353−357.
(19) Wang, J. Reticulated Vitreous Carbon-A New Versatile Electrode Material. *Electrochim. Acta* **1981**, *26*, 1721−1726.
(20) Blaedel, W. J.; Boyer, S. L. Electrochemical Characteristics of the Gold Micromesh Electrode. *Anal. Chem.* **1973**, *45*, 258−263.
(21) Langlois, S.; Coeuret, F. Flow-Through and Flow-By Porous Electrodes of Nickel Foam. I. Material Characterization. *J. Appl. Electrochem.* **1989**, *19*, 43−50.
(22) Newman, J.; Tiedemann, W. Porous-Electrode Theory with Battery Applications. *AIChE J.* **1975**, *21*, 25−41.
(23) Alkire, R.; Gracon, B. Flow-Through Porous Electrodes. *J. Electrochem. Soc.* **1975**, *122*, 1594−1601.
(24) Trainham, J. A.; Newman, J. A Flow-Through Porous Electrode Model: Application to Metal-Ion Removal from Dilute Streams. *J. Electrochem. Soc.* **1977**, *124*, 1528−1540.
(25) Walker, A. T. S.; Wragg, A. A. The Modeling of Concentration-Time Relationships in Recirculating Electrochemical Reactor Systems. *Electrochim. Acta* **1977**, *22*, 1129−1134.
(26) Sun, B.; Skyllas-Kazacos, M. Modification of Graphite Electrode Materials for Vanadium Redox Flow Battery Application—I. Thermal Treatment. *Electrochim. Acta* **1992**, *37*, 1253−1260.
(27) Zhang, G.; Sun, S.; Yang, D.; Dodelet, J. P.; Sacher, E. The Surface Analytical Characterization of Carbon Fibers Functionalized by H_2SO_4/HNO_3 Treatment. *Carbon* **2008**, *46*, 196−205.
(28) Wei, J.; Liang, P.; Huang, X. Recent Progress in Electrodes for Microbial Fuel Cells. *Bioresour. Technol.* **2011**, *102*, 9335−9344.
(29) Chen, J.-Z.; Liao, W.-Y.; Hsieh, W.-Y.; Hsu, C.-C.; Chen, Y.-S. All-Vanadium Redox Flow Batteries with Graphite Felt Electrodes Treated by Atmospheric Pressure Plasma Jets. *J. Power Sources* **2015**, *274*, 894−898.
(30) Weber, A. Z.; Mench, M. M.; Meyers, J. P.; Ross, P. N.; Gostick, J. T.; Liu, Q. Redox Flow Batteries: A Review. *J. Appl. Electrochem.* **2011**, *41*, 1137−1164.
(31) Leung, P.; Li, X.; Ponce De León, C.; Berlouis, L.; Low, C. T. J.; Walsh, F. C. Progress in Redox Flow Batteries, Remaining Challenges and Their Applications in Energy Storage. *RSC Adv.* **2012**, *2*, 10125−10156.
(32) Martínez-Huitle, C. A.; Rodrigo, M. A.; Sirés, I.; Scialdone, O. Single and Coupled Electrochemical Processes and Reactors for the Abatement of Organic Water Pollutants: A Critical Review. *Chem. Rev.* **2015**, *115*, 13362−13407.
(33) Cruz, M. A.; Ye, S.; Kim, M. J.; Reyes, C.; Yang, F.; Flowers, P. F.; Wiley, B. J. Multigram Synthesis of Cu-Ag Core−shell Nanowires Enables the Production of a Highly Conductive Polymer Filament for 3D Printing Electronics. *Part. Part. Syst. Charact.* **2018**, *35*, 1700385.
(34) Kim, M. J.; Alvarez, S.; Yan, T.; Tadepalli, V.; Fichthorn, K. A.; Wiley, B. J. Modulating the Growth Rate, Aspect Ratio, and Yield of Copper Nanowires with Alkylamines. *Chem. Mater.* **2018**, *30*, 2809−2818.
(35) Stewart, I. E.; Ye, S.; Chen, Z.; Flowers, P. F.; Wiley, B. J. Synthesis of Cu-Ag, Cu-Au, and Cu-Pt Core-Shell Nanowires and Their Use in Transparent Conducting Films. *Chem. Mater.* **2015**, *27*, 7788−7794.
(36) Chen, Z.; Ye, S.; Stewart, I. E.; Wiley, B. J. Copper Nanowire Networks with Transparent Oxide Shells That Prevent Oxidation without Reducing Transmittance. *ACS Nano* **2014**, *8*, 9673−9679.
(37) Schmal, D.; Van Erkel, J.; Van Duin, P. J. Mass Transfer at Carbon Fibre Electrodes. *J. Appl. Electrochem.* **1986**, *16*, 422−430.
(38) Delanghe, B.; Tellier, S.; Astruc, M. Mass Transfer to a Carbon or Graphite Felt Electrode. *Electrochim. Acta* **1990**, *35*, 1369−1376.
(39) Arenas, L. F.; Ponce de León, C.; Walsh, F. C. Engineering Aspects of the Design, Construction and Performance of Modular Redox Flow Batteries for Energy Storage. *J. Energy Storage* **2017**, *11*, 119−153.
(40) Lizarraga, D. S.; Bisang, J. M. Mass Transfer Studies at Iron Felts. *J. Appl. Electrochem.* **1996**, *26*, 1209−1215.
(41) Reichelt, E.; Heddrich, M. P.; Jahn, M.; Michaelis, A. Fiber Based Structured Materials for Catalytic Applications. *Appl. Catal., A* **2014**, *476*, 78−90.
(42) Rezk, K.; Forsberg, J.; Nilsson, L.; Berghel, J. Characterizing Flow Resistance in 3-Dimensional Disordered Fibrous Structures Based on Forchheimer Coefficients for a Wide Range of Reynolds Numbers. *Appl. Math. Model.* **2016**, *40*, 8898−8911.
(43) Walsh, F. C. *A First Course in Electrochemical Engineering*; The Electrochemical Consultancy: Romsey, U.K., 1993; pp 113−170.
(44) Arenas, L. F.; Ponce de León, C.; Walsh, F. C. 3D-Printed Porous Electrodes for Advanced Electrochemical Flow Reactors: A Ni/Stainless Steel Electrode and Its Mass Transport Characteristics. *Electrochem. Commun.* **2017**, *77*, 133−137.
(45) Stewart, I. E.; Kim, M. J.; Wiley, B. J. Effect of Morphology on the Electrical Resistivity of Silver Nanostructure Films. *ACS Appl. Mater. Interfaces* **2017**, *9*, 1870−1879.
(46) Waszczuk, P.; Zelenay, P.; Sobkowski, J. Surface Interaction of Benzoic Acid with a Copper Electrode. *Electrochim. Acta* **1995**, *40*, 1717−1721.
(47) Li, C. W.; Ciston, J.; Kanan, M. W. Electroreduction of Carbon Monoxide to Liquid Fuel on Oxide-Derived Nanocrystalline Copper. *Nature* **2014**, *508*, 504−507.
(48) Parkhouse, J. G.; Kelly, A. The Randon Packing of Fibers in Three Dimensions. *Proc. R. Soc. London, Ser. A* **1995**, *451*, 737−746.
(49) Choi, M. A.; Lee, M. H.; Chang, J.; Lee, S. J. Permeability Modeling of Fibrous Media in Composite Processing. *J. Non-Newtonian Fluid Mech.* **1998**, *79*, 585−598.
(50) Tomadakis, M. M.; Robertson, T. J. Viscous Permeability of Random Fiber Structures: Comparison of Electrical and Diffusional Estimates with Experimental and Analytical Results. *J. Compos. Mater.* **2005**, *39*, 163−188.
(51) Kok, M. D. R.; Gostick, J. T. Transport Properties of Electrospun Fibrous Membranes with Controlled Anisotropy. *J. Membr. Sci.* **2015**, *473*, 237−244.
(52) Hopkins, B. J.; Smith, K. C.; Slocum, A. H.; Chiang, Y.-M. Component-Cost and Performance Based Comparison of Flow and Static Batteries. *J. Power Sources* **2015**, *293*, 1032−1038.
(53) Barton, S. C.; Sun, Y.; Chandra, B.; White, S.; Hone, J. Mediated Enzyme Electrodes with Combined Micro- and Nanoscale Supports. *Electrochem. Solid-State Lett.* **2007**, *10*, B96−B100.
(54) Kjeang, E.; Michel, R.; Harrington, D. A.; Djilali, N.; Sinton, D. A Microfluidic Fuel Cell with Flow-Through Porous Electrodes. *J. Am. Chem. Soc.* **2008**, *130*, 4000−4006.
(55) González-García, J.; Bonete, P.; Expósito, E.; Montiel, V.; Aldaz, A.; Torregrosa-Maciá, R. Characterization of a Carbon Felt Electrode: Structural and Physical Properties Experimental Details. *J. Mater. Chem.* **1999**, *9*, 419−426.
(56) Walsh, F. C.; Arenas, L. F.; Ponce de León, C.; Reade, G. W.; Whyte, I.; Mellor, B. G. The Continued Development of Reticulated Vitreous Carbon as a Versatile Electrode Material: Structure, Properties and Applications. *Electrochim. Acta* **2016**, *215*, 566−591.
(57) Langlois, S.; Coeuret, F. Flow-Through and Flow-By Porous Electrodes of Nickel Foam. II. Diffusion-Convective Mass Transfer between the Electrolyte and the Foam. *J. Appl. Electrochem.* **1989**, *19*, 51−60.
(58) Bard, A. J.; Faulkner, L. R. *Electrochemical Methods: Fundamentals and Applications*, 2nd ed.; John Wiley & Sonc, Inc.: New York, 2001; pp 331−367.

DOI: 10.1021/acsnano.9b02058
ACS Nano 2019, 13, 6998−7009

(59) Reid, J. D.; David, A. P. Impedance Behavior of a Sulfuric Acid-Cupric Sulfate/Copper Cathode Interface. *J. Electrochem. Soc.* **1987**, *134*, 1389−1394.
(60) Zhang, S.; Li, X.; Chu, D. An Organic Electroactive Material for Flow Batteries. *Electrochim. Acta* **2016**, *190*, 737−743.
(61) Kim, M. J.; Flowers, P. F.; Stewart, I. E.; Ye, S.; Baek, S.; Kim, J. J.; Wiley, B. J. Ethylenediamine Promotes Cu Nanowire Growth by Inhibiting Oxidation of Cu(111). *J. Am. Chem. Soc.* **2017**, *139*, 277−284.
(62) Cahiez, G.; Chaboche, C.; Mahuteau-Betzer, F.; Ahr, M. Iron-Catalyzed Homo-Coupling of Simple and Functionalized Arylmagnesium Reagents. *Org. Lett.* **2005**, *7*, 1943−1946.
(63) Kim, M. J.; Seo, Y.; Cruz, M. A.; Wiley, B. J. Metal Nanowire Felt as a Flow-Through Electrode for High-Throughput Electrosynthesis. *ChemRxiv* **2018**, DOI: 10.26434/chemrxiv.7468703.v1, (accessed December 20, 2018) .

DOI: 10.1021/acsnano.9b02058
ACS Nano 2019, 13, 6998−7009